Published in final edited form as:
Ann Neurol. 2013 July ; 74(1): 128–139. doi:10.1002/ana.23897.

DRAVET SYNDROME PATIENT-DERIVED NEURONS SUGGEST A NOVEL EPILEPSY MECHANISM

Yu Liu, MD, PhD[1,*], **Luis F. Lopez-Santiago, PhD**[2,*], **Yukun Yuan, PhD**[2,*], **Julie M. Jones, MS**[3], **Helen Zhang, MS**[1], **Heather A. O'Malley, PhD**[2], **Gustavo A. Patino, PhD**[1,2,5], **Janelle E. O'Brien, PhD**[3], **Raffaella Rusconi, PhD**[2,9], **Ajay Gupta, MD**[8], **Robert C. Thompson, PhD**[4,5], **Marvin R. Natowicz, MD, PhD**[7,8], **Miriam H. Meisler, PhD**[3,5,*], **Lori L. Isom, PhD**[2,5,*], and **Jack M. Parent, MD**[1,5,6,*,+]

[1]Department of Neurology, University of Michigan Medical Center, Ann Arbor, MI

[2]Department of Pharmacology, University of Michigan Medical Center, Ann Arbor, MI

[3]Department of Human Genetics, University of Michigan Medical Center, Ann Arbor, MI

[4]Department of Psychiatry, University of Michigan Medical Center, Ann Arbor, MI

[5]Neuroscience Graduate Program, University of Michigan Medical Center, Ann Arbor, MI

[6]VA Ann Arbor Healthcare System, Ann Arbor, MI

[7]Genomic Medicine, Pediatric and Pathology, Laboratory Medicine Institutes, Cleveland Clinic, Cleveland Clinic Lerner College of Medicine, Cleveland, OH

[8]Neurological, Cleveland Clinic Lerner College of Medicine, Cleveland, OH

Abstract

OBJECTIVE—Neuronal channelopathies cause brain disorders including epilepsy, migraine and ataxia. Despite the development of mouse models, pathophysiological mechanisms for these disorders remain uncertain. One particularly devastating channelopathy is Dravet Syndrome (DS), a severe childhood epilepsy typically caused by de novo dominant mutations in the *SCN1A* gene encoding the voltage-gated sodium channel $Na_v1.1$. Heterologous expression of mutant channels suggests loss-of-function, raising the quandary of how loss of sodium channels underlying action potentials produces hyperexcitability. Mouse model studies suggest that decreased $Na_v1.1$ function in interneurons causes disinhibition. We sought to determine how mutant *SCN1A* affects human neurons using the induced pluripotent stem cell (iPSC) method to generate patient-specific neurons.

METHODS—Forebrain-like pyramidal- and bipolar-shaped neurons are derived from two DS subjects and three human controls by iPSC reprogramming of fibroblasts. DS and control iPSC-derived neurons are compared using whole-cell patch clamp recordings. Sodium current density and intrinsic neuronal excitability are examined.

RESULTS—Neural progenitors from DS and human control iPSCs display a forebrain identity and differentiate into bipolar- and pyramidal-shaped neurons. DS patient-derived neurons show increased sodium currents in both bipolar- and pyramidal-shaped neurons. Consistent with increased sodium currents, both types of patient-derived neurons show spontaneous bursting and

[+]Address correspondence to: Jack M. Parent, M.D., 5021 BSRB, 109 Zina Pitcher Place, Ann Arbor, MI 48109-2200, parent@umich.edu.
[9]Present address: German Center for Neurodegenerative Disease, Bonn, Germany
[*]These authors contributed equally

other evidence of hyperexcitability. Sodium channel transcripts are not elevated, consistent with a post-translational mechanism.

INTERPRETATION—These data demonstrate that epilepsy patient-specific iPSC-derived neurons are useful for modeling epileptic-like hyperactivity. Our findings reveal a previously unrecognized cell-autonomous epilepsy mechanism potentially underlying Dravet Syndrome, and offer a platform for screening new anti-epileptic therapies.

INTRODUCTION

Neuronal ion channelopathies due to genetic mutations comprise a constellation of central and peripheral nervous system disorders that manifest as epilepsy, migraine, ataxia, abnormal pain sensation or anosmia (Reviewed in[1,2]). Although the affected genes and involved neuronal subtypes are often known, the pathophysiological mechanisms underlying most of these disorders remain poorly understood. One such disorder is Dravet Syndrome (DS), a devastating form of epilepsy typically characterized by multiple pharmacoresistant seizure types, cognitive regression, ataxia and increased mortality[3, 4]. In more than 70% of cases, DS is caused by *de novo* mutations in the *SCN1A* gene which encodes the α subunit of the neuronal voltage-gated sodium channel $Na_v1.1$[5, 6]. Voltage-gated sodium channels underlie action potentials in excitable cells such as neurons and myocytes. DS is thought to be caused by *SCN1A* haploinsufficiency[7–9], raising the question of how a partial loss of sodium channel expression leads to neuronal hyperexcitability.

The effects of human DS *SCN1A* mutations or deletions of mouse *Scn1a* have been studied in heterologous expression systems and transgenic mouse models[10–13] but not in human neurons. The opportunity to study the effects of neuronal ion channel gene mutations in patient-specific neurons is now available using the induced pluripotent stem cell (iPSC) technique. This method involves reprogramming somatic cells, such as fibroblasts, using defined genetic factors to generate PSCs, and it has been accomplished in mice, humans and other species[14–17]. Recently, the effects of ion channel gene mutations have been studied in patient-specific cardiac myocytes generated from iPSCs, and these reports suggest that the patient-specific cells effectively model aspects of genetic cardiac arrhythmias[18–20]. However, this approach has not yet been applied to the study of human neuronal ion channelopathies.

Here we describe a splice donor site mutation[21] in the *SCN1A* gene of a 7-year-old DS patient. This mutation results in an abnormal transcript that skips exon 14. Expression of the mutant *SCN1A* cDNA in heterologous systems resulted in little to no $Na_v1.1$ protein and no detectable sodium current. We established human iPSC lines from the fibroblasts of this DS patient, one additional DS patient with a nonsense mutation, and three human controls. We generated forebrain-like neurons from DS and control iPSCs and found increased sodium current density in pyramidal- and bipolar-shaped neurons from both DS patients. This increased sodium current density was associated with spontaneous bursting and other evidence of epileptic-like hyperexcitability in DS patient neurons. Our results using patient-derived neurons suggest an unexpected pathophysiological mechanism underlying epilepsy in DS, and demonstrate that iPSC models of DS and other neuronal ion channelopathies will be useful for exploring disease pathogenesis and identifying novel therapies.

METHODS

Expression vectors

Human $Na_v1.1$ cDNA in pCDM8 was described previously[22]. The IVS14+3A>T mutation was introduced into this vector using the Quick Change XL Kit (Stratagene). Bacteria-

containing plasmids were grown at low temperature to reduce rearrangements as described[22]. Wildtype and mutant cDNAs were sequenced completely before use.

Western Blot Analysis

tsa-201 cells (maintained at 37°C with 5% CO_2) were cultured with DMEM/F12 medium supplemented with 10% heat inactivated fetal bovine serum (HI-FBS) and 100 U + 100 μg/ml penicillin/streptomycin (all from Invitrogen) in poly-D-Lysine-pretreated 10 cm dishes. Cells were mock-transgected or transfected at 60–70% confluency with pCDM8 vectors encoding wildtype or mutant human $Na_v1.1$ cDNA using the $CaPO_4$ method as described[22]. Transfected cells at 100% confluence were prepared for Western blot as described[23]. Proteins were separated by SDS-PAGE on 5% polyacrylamide gels, transferred to nitrocellulose, and analyzed using the SNAP i.d. apparatus (Millipore) per manufacturer's instructions. Primary antibodies: rabbit anti-pan sodium channel (1:1000, Sigma) and mouse anti-α-tubulin monoclonal (1:5000, Cedarlane Laboratories). Secondary antibodies: HRP-conjugated goat anti-rabbit or anti-mouse (1:2000, Pierce). Immunoreactive signals were quantified using ImageJ (NIH) and normalized to α-tubulin loading control.

Electrophysiological recordings

For recordings of cultured oocytes, human $Na_v1.1$ wildtype or IVS14+3A>T mutant cDNAs in pCDM8 were linearized with ScaI and mRNA synthesized using the T7 mMessage mMachine RNA Synthesis Kit (Ambion). Transcripts were injected into *Xenopus* oocytes and expressed sodium currents analyzed by two-electrode voltage clamp as described[24]. Published methods for mRNA analysis, frog maintenance, and oocyte retrieval were used[24]. iPSC-derived neurons were analyzed by whole-cell patch clamp recordings. Voltage clamp recordings were performed in the standard whole-cell configuration, using previously described conditions[25]. Isolated sodium currents were recorded from single neurons (bipolar or pyramidal) at RT (21–22 °C) in the presence of a bath solution containing (in mM): 120 NaCl, 1 $BaCl_2$, 2 $MgCl_2$, 0.2 $CdCl_2$, 1 $CaCl_2$, 10 HEPES, 20 TEA-Cl and 10 glucose (pH 7.35 with CsOH, Osmolarity: 300 – 305 mOsM). Fire-polished patch pipettes were filled with an internal solution containing (in mM): 1 NaCl, 150 N-methyl-D-glucamine, 10 EGTA, 2 $MgCl_2$, 40 HEPES, and 25 phosphocreatine-tris, 2 MgATP, 0.02 Na_2GTP, 0.1 Leupectin (pH 7.2 with H_2SO_4). All recordings were performed within 10–120 min after the culture medium was replaced by bath recording solution and the dish with cells was placed on the recording setup. For current-clamp recordings of action potentials in iPSC-derived neurons, patch pipettes were filled with internal solution consisting of (in mM): 135 K-gluconate, 4 NaCl, 0.5 $CaCl_2$, 10 HEPES, 5 EGTA, 2 Mg-ATP and 0.4 GTP (pH 7.3, adjusted with KOH). iPSCs were bathed in a solution consisting of (in mM): 115 NaCl, 2.5 KCl, 1 $MgCl_2$, 1.25 KH_2PO_4, 26 $NaHCO_3$, 2 $CaCl_2$, 10 HEPES and 10 D-glucose (pH 7.4, adjusted with NaOH). Action potentials were evoked from resting membrane potential by injection of a series of increasing 1 ms depolarizing currents (0.02 nA increments) beginning at subthreshold level until action potentials were consistently generated. The threshold potential was defined as the membrane potential at which these ascending current steps first initiated an action potential, and was measured at the end of the depolarizing pulse and the initiation point of the action potential. Repetitive spiking was evoked by injection of a 1500 ms depolarizing current (0.02 nA) from a holding potential at resting levels.

Generation of iPSCs and patient-specific neurons

DS patient and control skin biopsy-derived fibroblast cultures were obtained from the Cleveland Clinic under a protocol approved by the Institutional Review Board. Retroviral vectors (pMXs-Oct3/4, pMXs-Sox2, pMXs-Klf4, pMXs-c-Myc) were obtained from Addgene, and retroviral stocks generated using GP2-293 packaging cells (Clontech). To generate iPSCs from human fibroblasts (cultured in DMEM plus 10% fetal calf serum), two

rounds of viral transduction were performed on 30,000 fibroblasts and cells were incubated with virus for another 48 h. After 4 days, cells were passaged and cultured on mitotically-inactivated mouse embryonic fibroblasts (MEFS). iPSC colonies were manually picked and passaged. Undifferentiated iPSCs and human embryonic stem cells (hESCs; H7 line, Wicell Research Institute) were cultured and passaged on a MEF feeder layer with daily medium changes (DMEM/F12, 20% KSR, 1 mM L-glutamine, 0.1 mM non-essential amino acids, 0.1 mM β–mercaptoethanol [Sigma], and 4 ng/ml h-bFGF [from Invitrogen except as noted]) in dedicated incubators (37°C/5% CO2). For teratoma assays, DS and control iPSCs were cultured on MatriGel-coated dishes (BD Biosciences) in MEF-conditioned media. Cells were dissociated with trypsin, suspended in PBS (1×10^7 cells/ml), and subcutaneously injected (200 μl) in the upper hindlimbs of NOD scid gamma mice (The Jackson Laboratory). After 6–8 weeks, tumors were dissected and fixed with 4% PFA. Tissues were embedded in OCT, frozen, sectioned and stained with hematoxylin and eosin. To generate neural progenitor cells (NPCs), iPSCs were differentiated via EBs for 4–5 days and plated on Matrigel-coated dishes in NPC medium (DMEM/F12, N-2 supplement, 20 ng/ml b-FGF, non-essential amino acids, 2mM glutamine, and 2 μg/ml heparin [Sigma]). After 3 weeks, neural rosettes were isolated and NPCs expanded as floating neurospheres. For neuronal differentiation, neurospheres were dissociated with trypsin, and cells plated on Matrigel-coated dishes were cultured in differentiation medium lacking mitogens (Neurobasal plus B27 [Invitrogen], 10 ng/ml brain-derived neurotrophic factor and neurotrophin-3 [PeproTech]) for 2 months.

RT-PCR and gene expression profiling

Total RNA was extracted from iPSCs, hESCs, fibroblasts and neural progeny with the RNeasy Mini or Micro kit (Qiagen) and DNAse I treatment. First strand cDNA synthesis was done from 2 μg of total RNA using Superscript III reverse transcriptase (Invitrogen) and random hexamers according to the manufacturer's instructions. PCR was performed in 25 μl reactions containing 200 nM each of forward and reverse primers, 1xPCR buffer, Taq DNA polymerase and cDNA template. PCR primer sequence and annealing temperature are provided in Supplementary Table 1. For RT-PCR of sodium channel genes, cDNA was synthesized from 250 ng of total RNA using the Superscript First Strand cDNA Synthesis Kit (Invitrogen). PCR was performed in 25-μl reactions containing 500 nM each of forward and reverse primers, 1xPCR buffer, 200 nM dNTPs, 1 unit Taq DNA polymerase (Promega) and cDNA template. Amplification was carried out with an initial 3 min denaturation at 94°C, followed by 35 cycles of 45 sec at 94°C, 45 sec at 60°C, and 45 sec at 72°C, and terminating with a 10 minute extension reaction at 72°C. The forward primer *SCN1A*x13 is located in exon 13 and the reverse primer, *SCN1A*x15 is located in exon 15; this primer pair amplifies a 343 bp fragment from the wildtype transcript and a 169 bp fragment from the DS1 transcript lacking exon 14 (174 bp in length). To obtain gene-specific amplification of sodium channel transcripts, primer pairs were designed with the 3' terminus of one or both primers terminating on 1 to 2 bases that are specific to one gene in the sodium channel family (Supplementary Table 1). Sodium channel primers designated F and R are located in the penultimate and final exon of each gene, respectively. Amplified fragments were sequenced to confirm specificity. Quantitative RT-PCR for exogenous Oct4, Klf4, Sox2 and c-Myc was performed with the SYBR Green qPCR reagent (Applied Biosystems) containing 200 nM each of forward and reverse primers and template using a Bio-Rad iCycler PCR machine. For microarrays, total RNA (400 ng) was labeled with the Total Prep RNA amplification kit (Ambion), and biotin-labeled complementary RNA (750 ng) prepared for hybridization to the Illumina HumanHT-12 v4 Expression BeadChip. Chips were washed, labeled with Cy3, scanned into an Illumina BeadArray Reader and analyzed with GenomeStudio (Illumina, Inc).

Immunocytochemistry and microscopy

Cultures were fixed with 4% paraformaldehyde for immunocytochemistry. For immunostaining involving nuclear and cytoplasmic proteins, cells were permeabilized with 0.2% Triton X-100. Antibodies used were: Pax6 (1:100, DHSB), Musashi (1:500, Chemicon), Forse 1 (1:1,000 Chemicon), Otx2 (1:500, R&D) En1 (1:500, Chemicon), Oct3/4 (1:200, Santa Cruz), Nanog (1:500, Chemicon), SSEA-4 (1:200, Chemicon), SMA (1:1000, Sigma), Alpha-fetoprotein (1:500, Dako), β-III-tubulin (TuJ1 clone, 1:2,000, COVANCE), MAP 2ab (1:1,000, Sigma), Tbr-1 (1:400 Abcam), GABA (1:3,000, Sigma), VGLUT1 (1:4,000, Chemicon), Parvalbumin (1:400, Abcam), Calretinin (1:2,000 Chemicon), Calbindin (1:500, Abcam), Somatostatin (1:300, Millipore), Tyrosine Hydroxylase (1:400, Chemicon), Vimentin (1:1000, MBL), GFAP (1:1000, Sigma) and S-100β (1:400, Swant). Conjugated secondary antibodies were applied and nuclei counterstained with bisbenzimide. Stained cells were viewed and imaged using epifluorescence microscopy (Leica DSM*IRB*) and a SPOT-RT digital camera.

Statistical Analysis

Voltage clamp data were tested for normality using the Shapiro-Wilk test. Continuous variables with normal distribution were compared using two-tailed Student's *t* test or ANOVA. Current clamp data from patient and control iPSCs were compared using Student *t* test. Values were considered statistically significant at $p \leq 0.05$.

RESULTS

A novel loss-of-function *SCN1A* splice site mutation in a 7-year-old patient with DS

The first subject's seizures began at age 9 months, his development subsequently regressed and he experienced multiple types of pharmacoresistant seizures. Diagnostic sequencing identified a heterozygous splice donor site mutation IVS14+3A>T (Fig. 1A). This mutation substitutes a pyrimidine at the important +3 position that is occupied by a purine (G or A) at >95% of human splice sites. The subject's parents do not carry the mutation (data not shown), consistent with a *de novo* pathogenic mutation, as is frequently seen in DS[6]. RT-PCR of RNA from the cultured fibroblasts using primers in exon 13 and exon 15 yields two major products, the product of the wildtype allele that contains exon 14 and the mutant product that skips exon 14 (Fig. 1B). The identity of RT-PCR products was confirmed by sequencing. Using primers in exon 11 and exon 15, a less abundant transcript that skips both exons 13 and 14 was detected (data not shown). Since exon 14 contains 174 bp, the open reading frame is maintained in the mutant transcript but the predicted protein product has deletion of transmembrane segments 2 and 3 in domain 2, with predicted loss of channel function (Fig. 1C).

To test the function of the mutant channel, we expressed either wildtype human *SCN1A* cDNA or a cDNA lacking the codons from exon 14 in *Xenopus* oocytes and recorded whole-cell sodium currents under voltage clamp. Consistent with previous findings[26], injection of RNA encoding wild-type human *SCN1A* resulted in the expected whole-cell sodium currents (Fig. 1Di). In contrast, injection of the mutant RNA failed to produce any detectable current (Fig. 1Dii). We next transfected mammalian tsa-201 cells with cDNA encoding wild-type or mutant *SCN1A* and performed immunoblots of cell lysates. Robust expression of $Na_v1.1$ channel protein was obtained with wild-type *SCN1A*, but the mutant $Na_v1.1$ protein was not detectable above background (Fig. 1E, F), although we cannot exclude expression of a markedly truncated, non-functional protein. Together, these findings demonstrate that the mutant protein is unstable and does not produce functional channels at the cell membrane. We also expressed mutant and wild-type channel alone or in combination in tsa-201 cells and found no current expressed by mutant channel alone, and

no influence of the mutant channel on wild-type current to suggest a dominant-negative effect (data not shown). Thus this patient is heterozygous for a null allele of *SCN1A*, as characteristic for DS[6].

Generation of DS patient and control iPSCs and neurons

Heterologous expression systems provide only limited data regarding the actual function of a mutant channel in the cells of physiological interest that, in the case of epilepsy, are forebrain neurons. Moreover, differences in genetic background both between and within species may substantially influence neuronal ion channel function[27]. In order to characterize the net *in vivo* effect of the *SCN1A* mutation in the genomic background of genetic modifiers, we chose to study the functional effects of DS patient *SCN1A* mutations using the subjects' own neurons via the iPSC method. Primary fibroblasts were derived from skin biopsies obtained from two DS subjects (both age 7 years) and three unaffected controls (ages 1, 10 and 25 years), and were reprogrammed by retroviral-mediated gene transfer of Oct4, Sox2, Klf4, and cMyc[14,15]. We initially worked with fibroblasts from the DS patient carrying the IVS14+3A>T mutation described above, and the majority of our results are from this subject (DS1). We subsequently reprogrammed cultured fibroblasts from an additional subject with DS (DS2) who has a c.975T>A *SCN1A* nonsense mutation in tyrosine codon 325, resulting in the premature termination codon TAA (Y325X). This mutation truncates the four-domain sodium channel protein within the pore loop of domain 1, resulting in a predicted loss of channel activity. A *de novo* missense mutation in the same codon, Y325C, was previously observed in a patient with Dravet Syndrome (*SCN1A* Variant Database, http://www.molgen.vib-ua.be/SCN1AMutations).

Colonies with hESC-like morphology emerged within 10–14 days after fibroblast reprogramming (Fig. 2A, B) and by 30 days they displayed the morphology of pluripotent stem cells similar to a simultaneously cultured H7 hESC line (Fig. 2C, D). At 3–4 weeks after reprogramming, colonies were manually picked and individually passaged onto irradiated MEF feeder cells. RT-PCR analysis of *SCN1A* showed that the mutant transcript lacking exon 14 was expressed in DS1 patient-derived iPSCs (Supplementary Fig. 1A). Consistent with successful reprogramming into iPSCs, cells from four lines (from DS1, DS2 and two controls) were injected into immunocompromised mice and formed teratomas (Supplementary Fig. 1B and data not shown). Reprogrammed iPSCs lost expression of a fibroblast associated antigen, TE-7 (data not shown), and all iPSC clones from DS patients and controls, unlike the fibroblasts, continuously expressed pluripotency markers including Nanog, Oct3/4, SSEA4, alkaline phosphatase and others (Fig. 2E–H; Supplementary Fig. 1C). We also compared the global gene expression profiles among undifferentiated patient and control iPSCs, H7 cells, and fibroblasts that were not reprogrammed. As expected, the iPSCs showed a gene expression profile that was much more similar to H7 hESCs than to the original fibroblasts from which they were derived (Supplementary Fig. 1D). RT-PCR for the exogenous transcription factor transgenes used for reprogramming showed marked downregulation after fibroblasts were converted to iPSCs (Supplementary Fig. 1E). Also consistent with a pluripotent cell phenotype, control and patient-derived iPSCs could be differentiated through embryoid bodies (EBs) to give rise to cells comprising all three embryonic germ layers (Fig. 2I–L and data not shown).

Because forebrain neurons are the affected cells that cause disease in DS, we directed the differentiation of patient and control iPSCs toward a forebrain neural progenitor cell (NPC) phenotype. Five-day-old EBs were cultured to generate NPCs. Early NPCs displayed a neural rosette morphology and expressed forebrain-specific regionalization markers but not more caudal CNS markers or a pluripotency gene (Fig. 3A–C; Supplementary Fig. 2A–E). Neural rosettes were manually picked, passaged, dissociated and differentiated to generate neurons and glia. Early differentiating cells (2–7 weeks) expressed neuronal antigens

including neuron-specific β-tubulin and microtubule-associated protein-2 (MAP2) (Fig. 3E–F; Supplementary Fig. 3B–D), and exhibited increased expression of five voltage-gated sodium channels predominantly expressed in neurons (Supplementary Fig. 3A). Approximately 80–90% of the neurons displayed a bipolar morphology and expression of gamma-aminobutyric acid (GABA) characteristic of an interneuron phenotype, while about 10% were pyramidal shaped and expressed the vesicular glutamate transporter-1 (VGLUT1) (Fig. 3E–G) and the forebrain pyramidal cell marker Tbr1 (Supplementary Fig. 2E). Rare cells expressed tyrosine hydroxylase (TH) indicative of a monoaminergic cell type (Fig. 3H). To determine the types of interneurons generated from the iPSCs, we immunostained for different forebrain interneuron subtypes and found subsets of cells expressing calretinin, calbindin, parvalbumin or somatostatin (Supplementary Fig. 3B–D and data not shown). A predominance of interneurons generated by pluripotent stem cells is not unusual[28–30], although other culture conditions produce more pyramidal neurons (e.g.,[31]). With longer culture durations (7–12 weeks) there was appearance of substantial numbers of glia that expressed glial fibrillary acidic protein, S100 β and vimentin (data not shown). Although neuronal RNA splicing may vary from that of other cell types, we found that iPSC-derived neurons (herein called induced neurons) from subject DS1 with the IVS14+3A>T mutation retained the abnormal exon 14 splicing of *SCN1A* described above for fibroblasts and iPSCs (Supplementary Fig. 1A).

Increased sodium current density and neuronal excitability in *SCN1A* mutant neurons

To examine whether induced neurons from DS subjects and controls differed in ways that may predispose to epileptic seizures, we performed whole-cell voltage- and current-clamp recordings. We first recorded sodium currents and measured current densities under voltage clamp in induced neurons that were differentiated for 5–7 days. As expected, given the upregulation of voltage-gated sodium channel mRNAs (Supplementary Fig. 3A), both bipolar- and pyramidal-shaped neurons from DS1 mutant and controls showed typical sodium currents (Supplementary Fig. 4). No significant differences in sodium current densities were observed between DS1 and control induced neurons at this time point, or between bipolar- and pyramidal-shaped neurons within groups (Supplementary Fig. 4B).

We next measured sodium current densities of induced neurons after differentiation for 3–5 weeks. Neurons with both pyramidal- and bipolar-shaped morphologies from DS subjects and controls showed sodium currents that were blocked with the addition of 300 nM tetrodotoxin (TTX; Fig. 4; Supplementary Fig. 4C), a finding consistent with neuronal TTX-sensitive sodium currents. However, we observed significantly increased (~2-fold) mean sodium current densities in 3–5-week-differentiated DS mutant neurons with both pyramidal and bipolar morphologies derived from DS1 compared to controls (Fig. 4). Induced mutant neurons of both morphologies derived from DS2 exhibited ~3-fold increases in sodium current density compared to controls (Fig. 4). Sodium current densities in control neurons remained similar to the levels measured at 5–7 days. No significant differences in sodium current densities were present between bipolar- and pyramidal-shaped neurons within groups. In contrast to current density, the voltage-dependence and kinetics of current activation and inactivation were not different between control and mutant induced neurons (Supplementary Fig. 4D–E).

To examine whether the increase in sodium current density was associated with altered neuronal excitability of mutant neurons, we recorded action potentials from DS mutant and control induced neurons differentiated for 3–7 weeks under current clamp recording conditions. In both mutant and control neurons, action potentials were evoked with stimulation after four weeks of differentiation, with more consistently produced repetitive firing by five weeks. DS1- or DS2-derived mutant induced bipolar and pyramidal neurons differentiated for 5–7 weeks exhibited a significantly reduced threshold for action potential

generation and increased repetitive firing frequency compared to controls (Fig. 5; Table 1). Moreover, mutant pyramidal- and bipolar-shaped neurons frequently displayed spontaneous repetitive firing and bursting activity that were almost never observed in control neurons (Fig. 5; Supplementary Fig. 5; Table 2). Changes in neuronal excitability in mutant pyramidal and bipolar neurons from DS1 and DS2 were virtually identical, and pooled data for the two subjects are shown in Tables 1 and 2. Thus, both loss-of-function mutations in *SCN1A* increased neuronal excitability. To confirm that sodium current densities remained increased in DS induced neurons after 5–7 weeks of differentiation, we measured current densities under voltage clamp in these more mature neurons. Sodium current densities in bipolar- and pyramidal-shaped DS1 induced neurons differentiated for 5–7 weeks remained significantly increased compared to control induced neurons of the same maturity (Supplementary Fig. 6), and no significant differences were present between bipolar- and pyramidal-shaped neurons within groups.

Consistent with the increased sodium current densities shown in Fig. 4 and Supplementary Fig. 6, the mutant neurons also displayed more depolarized resting membrane potentials than those of the control neurons, although the difference was only significant for bipolar-shaped cells (Table 1). However, there were no differences in other intrinsic membrane electrical properties including membrane capacitance and input resistance between DS and control induced neurons. All of the current and voltage clamp recordings were consistent for three sublines from DS1, 2 sublines from DS2, and all three controls. Taken together, these data suggest that pyramidal- and bipolar-shaped DS mutant induced neurons are hyperexcitable, a result consistent with an *in vitro* epileptic-like phenotype.

Quantitation of sodium channel transcripts—The level of sodium channel transcripts increases during the transition from iPSCs to derived neurons (Supplementary Fig. 3A). To determine whether there was transcriptional up-regulation of one or more sodium channel genes in induced neurons from DS patients compared to controls, we carried out RT-PCR using gene-specific primers for the 5 sodium channel genes that are expressed in these cells: *SCN1A, SCN2A, SCN3A, SCN8A* and *SCN9A*. None of the sodium channel transcripts were elevated in patient derived neurons compared with control neurons (Fig. 6). These data indicate that the elevated sodium current density in patient-derived neurons results from a post-transcriptional mechanism.

DISCUSSION

We used the iPSC method to compare the physiological properties and sodium channel subunit expression of forebrain-like neurons from 2 DS subjects and 3 human controls. Voltage-clamp recordings initially (5–7 days) showed sodium current densities that were not significantly different between induced neurons from DS subjects and controls. The neurons were very immature and lacked action potentials at this early stage, however, with further maturation *in vitro* to functional neurons, DS induced neurons developed significantly greater sodium current densities than those of controls. These findings were present in both putative excitatory pyramidal-shaped neurons and inhibitory neurons with bipolar morphology. Current clamp recordings showed that DS induced neurons of both morphologies were hyperexcitable compared to controls, with significantly reduced thresholds for action potential generation and increased firing frequency, as well as spontaneous repetitive firing and bursting behavior. These findings indicate that DS iPSC-derived neurons model an epileptic-like phenotype with *in vitro* seizure-like activity.

The functional effects of *SCN1A* mutations were initially explored using voltage clamp recordings in heterologous expression systems such as *Xenopus* oocytes or non-neuronal mammalian cell lines[10,11]. An inconsistent mixture of loss-of-function and gain-of-function

effects of individual mutations was obtained with this approach[6,9,32]. The advantages of the iPSC approach over these heterologous expression systems are underscored in the present study. The mutant channels are present in the natural host cells without the need for transfection. In addition, the patient genetic background is maintained and therefore the properties of the induced neurons reflect the net effect of the mutation and genetic modifiers.

Mouse models of DS have been generated by targeted deletion of mouse *Scn1a* and knock-in of a human *SCN1A* premature truncation mutation causing DS[12,13]. Homozygous and heterozygous *Scn1a* null mice display spontaneous seizures; the homozygotes are ataxic and die at the beginning of the third postnatal week, while more than half of the heterozygotes survive to adulthood[12]. Voltage clamp recordings from acutely dissociated hippocampal neurons derived from heterozygous and homozygous *Scn1a* null mice revealed decreased sodium current densities in putative interneurons with bipolar morphology, but not in neurons with pyramidal morphology[12,13]. The interneurons also showed decreased current-induced repetitive firing and reduced action potential amplitudes. A compensatory upregulation of $Na_v1.3$ was seen in homozygous and heterozygous *Scn1a* null mice, but this was not sufficient to restore normal sodium currents in putative interneurons. Similarly, studies using a knock-in mouse model of DS revealed decreased bursting of fast-spiking interneurons in *in vitro* cortical slices from heterozygotes[13]. Together, findings from these mouse DS models, along with a more recent study using mice with conditional deletion of *Scn1a* in interneuron progenitors[33], led to the "interneuron hypothesis" of epileptogenesis in DS whereby decreased excitability of inhibitory interneurons leads to network hyperexcitability and seizures.

Our data from human mutant DS iPSC neurons differ substantially from those in the murine DS models and do not support the idea of an interneuron-specific decrease in excitability. We observed *increased* sodium current densities and *hyperexcitability* of both bipolar-shaped putative inhibitory interneurons and putative pyramidal neurons, suggesting an alternative mechanism of seizure generation that is cell-autonomous and not dependent upon inhibitory innervation. Such a mechanism is supported by more recent data from a mouse *Scn1a* heterozygous knockout DS model, in which sodium current density in pyramidal neurons is initially unchanged, but then significantly increases by the fourth week of life[34].

Our findings raise two critical questions. First, what is the cause of the increased sodium current density in DS patient-specific neurons? We found that DS and control sodium currents were similar in immature neurons, and that sodium currents increase in DS neurons as they mature. These data suggest a cell autonomous, homeostatic-like mechanism that overcompensates, perhaps by overexpression of a different voltage-gated sodium channel α-subunit or a pro-excitatory change in another ion channel. We did not observe increases in other voltage-gated sodium channel α subunit expression at the mRNA level, suggesting that if there is any compensatory increase in these subunits, it would be through post-transcriptional mechanisms or altered subcellular targeting.

Second, how might the similar changes that we see in both interneurons and pyramidal cells cause epilepsy? The most plausible explanation is that increased excitability of both principal and inhibitory neurons leads to network hyperexcitability or synchronization sufficient to produce seizures and cognitive dysfunction. This effect might be analogous to the administration of a chemoconvulsant, such as kainic acid, that increases the activity of both inhibitory and excitatory neurons with the net outcome of seizure generation. Another possibility is that early hyperexcitability of neurons during embryonic development leads to abnormal neuronal integration and resultant network hyperexcitability. Some studies have found minor malformations of cortical development in DS but others have not (reviewed in[35]). Another issue relates to the clinical phenomena of worsening seizures in many DS

subjects treated with sodium-channel blocking anticonvulsants such as lamotrigine[36]. This phenomenon is not easily explained by a mechanism involving compensatory increases in sodium currents, as proposed here. However, there is currently no direct evidence in any DS model system explaining this clinical finding, which is not seen in all DS subjects. Further, the "interneuron hypothesis" put forward based on the initial DS mouse model data also does not provide an adequate explanation. For example, the argument is made that if DS interneurons specifically lack $Na_v1.1$ resulting in decreased sodium current DS, they would be affected to a greater extent than wildtype neurons by sodium channel blockers. However, one might just as well argue that pyramidal cells would be more affected in this situation because they have higher levels of sodium current, more channels to block, and thus the drugs should work better. Additional caveats include the complicated network effects generated by other likely homeostatic mechanisms at play, and the often ignored issue that all of these anticonvulsants have multiple mechanisms of action.

Human iPSCs provide a remarkable experimental platform for understanding disease mechanisms and screening therapeutic drugs using patient-specific cells. For example, three recent studies reported the generation of patient-specific iPSCs and cardiac myocytes from subjects with two different forms of congenital long QT syndrome due to potassium channel gene mutations[18,19], and a third form of long QT syndrome due to a calcium channel mutation[20]. The patient-specific cardiac myocytes modeled the disease phenotypes remarkably well, with action potential prolongation, increased *in vitro* arrhythmogenic potential, and responses to pharmacological agents that influence cardiac rhythmicity. Several patient-specific iPSC lines have been generated as models of other neurological diseases[17,37–39], but the mechanistic information derived thus far has been limited. A general limitation of the method is the possible impact of factors specific to the culture conditions or the state of differentiation of the iPSC-derived neurons. Nonetheless, our patient-specific DS model suggests that disease-causing neuronal ion channelopathies are amenable to modeling with iPSC-derived neurons. In addition to providing new insight into disease pathogenesis, the iPSC approach should prove an invaluable tool to evaluate candidate pharmacological agents using patient-specific cells.

Supplementary Material

Refer to Web version on PubMed Central for supplementary material.

Acknowledgments

This work was supported by grants from the NIH to M.H.M. (RC1NS068684) and to L.L.I. (NS064245 and NS076752), the American Epilepsy Society to J.M.P., a grant from the University of Michigan Rare Disease Initiative to L.L.I., a fellowship from the Epilepsy Foundation to G.A.P., from NIH T32HL007853 to the University of Michigan Cardiovascular Center for H.O.M., and from NIGMS Genetics Predoctoral Training Grant T32 for J.E.O. We thank K. Sue O'Shea for generous assistance with the teratoma assays.

References

1. Catterall WA, Dib-Hajj S, Meisler MH, Pietrobon D. Inherited neuronal ion channelopathies: new windows on complex neurological diseases. J Neurosci. 2008; 28:11768–11777. [PubMed: 19005038]
2. Kullmann DM, Waxman SG. Neurological channelopathies: new insights into disease mechanisms and ion channel function. J Physiol. 2010; 588:1823–1827. [PubMed: 20375141]
3. Dravet C, Bureau M, Oguni H, Fukuyama Y, Cokar O. Severe myoclonic epilepsy in infancy: Dravet syndrome. Adv Neurol. 2005; 95:71–102. [PubMed: 15508915]

4. Guerrini R, Aicardi J. Epileptic encephalopathies with myoclonic seizures in infants and children (severe myoclonic epilepsy and myoclonic-astatic epilepsy). J Clin Neurophysiol. 2003; 20:449–461. [PubMed: 14734934]
5. Claes L, et al. De novo mutations in the sodium-channel gene SCN1A cause severe myoclonic epilepsy of infancy. Am J Hum Genet. 2001; 68:1327–1332. [PubMed: 11359211]
6. Meisler MH, Kearney JA. Sodium channel mutations in epilepsy and other neurological disorders. J Clin Invest. 2005; 115:2010–2017. [PubMed: 16075041]
7. Kanai K, et al. Effect of localization of missense mutations in SCN1A on epilepsy phenotype severity. Neurology. 2004; 63:329–334. [PubMed: 15277629]
8. Ceulemans BP, Claes LR, Lagae LG. Clinical correlations of mutations in the SCN1A gene: from febrile seizures to severe myoclonic epilepsy in infancy. Pediatr Neurol. 2004; 30:236–243. [PubMed: 15087100]
9. Catterall WA, Kalume F, Oakley JC. NaV1.1 channels and epilepsy. J Physiol. 2010; 588:1849–1859. [PubMed: 20194124]
10. Spampanato J, Escayg A, Meisler MH, Goldin AL. Functional effects of two voltage-gated sodium channel mutations that cause generalized epilepsy with febrile seizures plus type 2. J Neurosci. 2001; 21:7481–7490. [PubMed: 11567038]
11. Lossin C, et al. Epilepsy-associated dysfunction in the voltage-gated neuronal sodium channel SCN1A. J Neurosci. 2003; 23:11289–11295. [PubMed: 14672992]
12. Yu FH, et al. Reduced sodium current in GABAergic interneurons in a mouse model of severe myoclonic epilepsy in infancy. Nat Neurosci. 2006; 9:1142–1149. [PubMed: 16921370]
13. Ogiwara I, et al. Na(v)1.1 localizes to axons of parvalbumin-positive inhibitory interneurons: a circuit basis for epileptic seizures in mice carrying an Scn1a gene mutation. J Neurosci. 2007; 27:5903–5914. [PubMed: 17537961]
14. Takahashi K, Yamanaka S. Induction of pluripotent stem cells from mouse embryonic and adult fibroblast cultures by defined factors. Cell. 2006; 126:663–676. [PubMed: 16904174]
15. Takahashi K, et al. Induction of pluripotent stem cells from adult human fibroblasts by defined factors. Cell. 2007; 131:861–872. [PubMed: 18035408]
16. Yu J, et al. Induced pluripotent stem cell lines derived from human somatic cells. Science. 2007; 318:1917–1920. [PubMed: 18029452]
17. Park IH, et al. Disease-specific induced pluripotent stem cells. Cell. 2008; 134:877–886. [PubMed: 18691744]
18. Moretti A, et al. Patient-specific induced pluripotent stem-cell models for long-QT syndrome. N Engl J Med. 2010; 363:1397–1409. [PubMed: 20660394]
19. Itzhaki I, et al. Modelling the long QT syndrome with induced pluripotent stem cells. Nature. 2011; 471:225–229. [PubMed: 21240260]
20. Yazawa M, et al. Using induced pluripotent stem cells to investigate cardiac phenotypes in Timothy syndrome. Nature. 2011; 471:230–234. [PubMed: 21307850]
21. Harkin LA, et al. The spectrum of SCN1A-related infantile epileptic encephalopathies. Brain. 2007; 130:843–852. [PubMed: 17347258]
22. Rusconi R, et al. Modulatory proteins can rescue a trafficking defective epileptogenic Nav1.1 Na+ channel mutant. J Neurosci. 2007; 27:11037–11046. [PubMed: 17928445]
23. Patino GA, et al. A functional null mutation of SCN1B in a patient with Dravet syndrome. J Neurosci. 2009; 29:10764–10778. [PubMed: 19710327]
24. Fein AJ, Meadows LS, Chen C, Slat EA, Isom LL. Cloning and expression of a zebrafish SCN1B ortholog and identification of a species-specific splice variant. BMC Genomics. 2007; 8:226. [PubMed: 17623064]
25. Lopez-Santiago LF, et al. Sodium channel beta2 subunits regulate tetrodotoxin-sensitive sodium channels in small dorsal root ganglion neurons and modulate the response to pain. J Neurosci. 2006; 26:7984–7994. [PubMed: 16870743]
26. Smith RD, Goldin AL. Functional analysis of the rat I sodium channel in xenopus oocytes. J Neurosci. 1998; 18:811–820. [PubMed: 9437003]

27. Frankel WN. Genetics of complex neurological disease: challenges and opportunities for modeling epilepsy in mice and rats. Trends Genet. 2009; 25:361–367. [PubMed: 19665252]
28. Erceg S, et al. Differentiation of human embryonic stem cells to regional specific neural precursors in chemically defined medium conditions. PLoS One. 2008; 3:e2122. [PubMed: 18461168]
29. Kim JE, et al. Investigating synapse formation and function using human pluripotent stem cell-derived neurons. Proc Natl Acad Sci U S A. 2011; 108:3005–3010. [PubMed: 21278334]
30. Koch P, Opitz T, Steinbeck JA, Ladewig J, Brustle O. A rosette-type, self-renewing human ES cell-derived neural stem cell with potential for in vitro instruction and synaptic integration. Proc Natl Acad Sci U S A. 2009; 106:3225–3230. [PubMed: 19218428]
31. Shi Y, Kirwan P, Livesey FJ. Directed differentiation of human pluripotent stem cells to cerebral cortex neurons and neural networks. Nat Protoc. 2012; 7:1836–1846. [PubMed: 22976355]
32. Mantegazza M. Dravet syndrome: insights from in vitro experimental models. Epilepsia. 2011; 52(Suppl 2):62–69. [PubMed: 21463283]
33. Cheah CS, et al. Specific deletion of NaV1.1 sodium channels in inhibitory interneurons causes seizures and premature death in a mouse model of Dravet syndrome. Proc Natl Acad Sci U S A. 2012; 109:14646–14651. [PubMed: 22908258]
34. Mistry A, Miller A, Thompson C, Kearney J, George AL. Strain and age-dependent differences in hippocampal neuron sodium current densities in a mouse model of Dravet Syndrome. Soc. Neurosci. Abstr. 2012
35. Guerrini R, Striano P, Catarino C, Sisodiya SM. Neuroimaging and neuropathology of Dravet syndrome. Epilepsia. 2011; 52(Suppl 2):30–34. [PubMed: 21463276]
36. Guerrini R, et al. Lamotrigine and seizure aggravation in severe myoclonic epilepsy. Epilepsia. 1998; 39:508–512. [PubMed: 9596203]
37. Dimos JT, et al. Induced pluripotent stem cells generated from patients with ALS can be differentiated into motor neurons. Science. 2008; 321:1218–1221. [PubMed: 18669821]
38. Ebert AD, et al. Induced pluripotent stem cells from a spinal muscular atrophy patient. Nature. 2009; 457:277–280. [PubMed: 19098894]
39. Marchetto MC, et al. A model for neural development and treatment of Rett syndrome using human induced pluripotent stem cells. Cell. 2010; 143:527–539. [PubMed: 21074045]

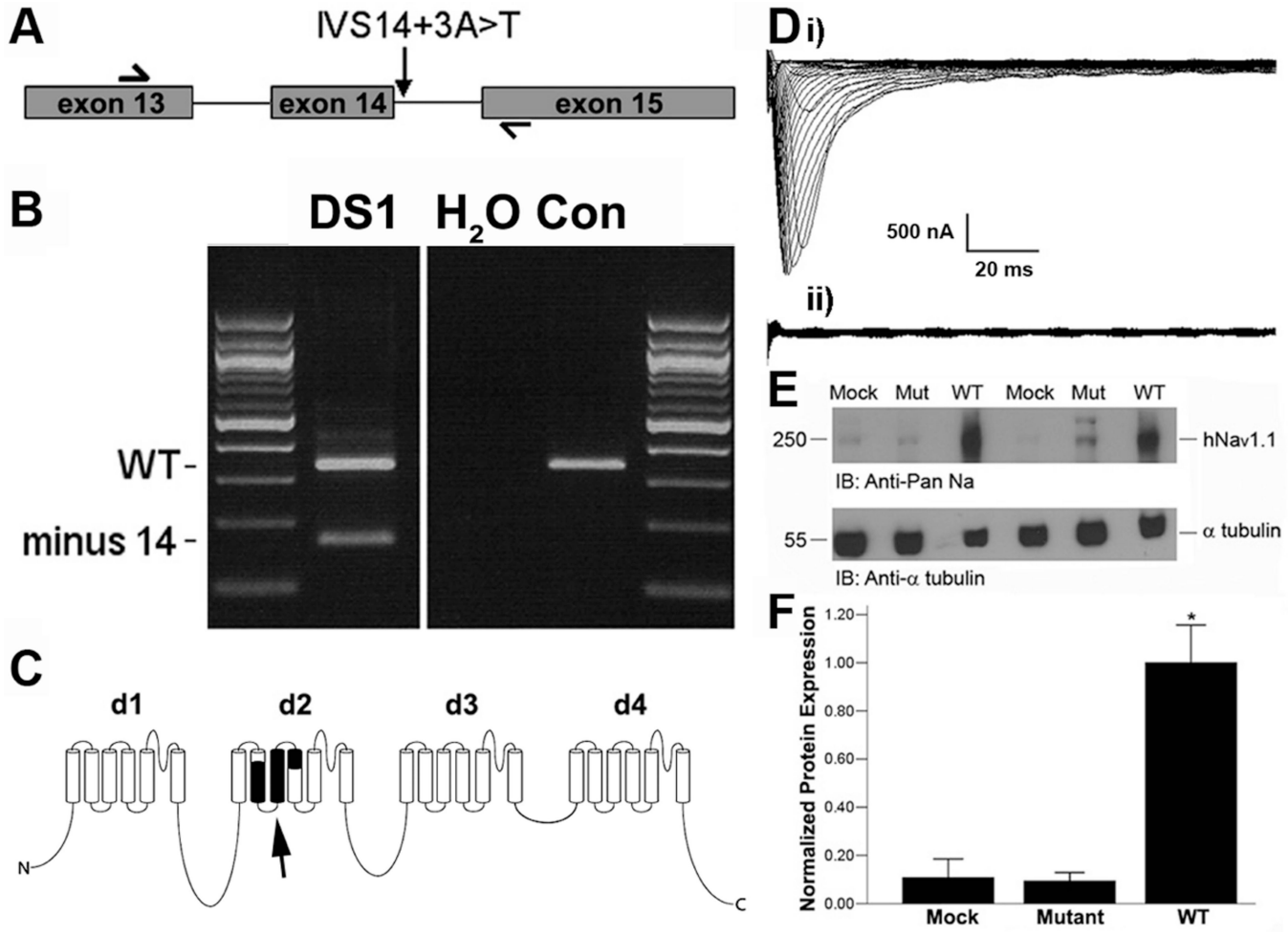

Figure 1.

SCN1A transcripts in fibroblast cultures from patient DS1 (splice donor site mutation IVS14+3 A>T in intron 14). (A) The mutation is located 3 bp downstream of exon 14. PCR primers are located in exons 13 and 15. (B) RT-PCR products from DS patient and control fibroblasts. In addition to the wildtype product of 340 bp that contains exon 14, the patient's fibroblasts produce a smaller product that skips exon 14, as confirmed by sequencing. (C) Diagram of $Na_v1.1$ channel protein α subunit with exon 14 residues in black (arrow). (D) Traces of two electrode voltage-clamp recordings from *Xenopus* oocytes injected with RNA of human wildtype (i) or IVS14+3A>T DS mutant (ii) *SCN1A*. Only the wildtype generates sodium current. Scale bar: vertical = 500 nA; horizontal = 20 ms. (E) Immunoblots of tsa-201 cells transfected with wildtype or IVS14+3A>T mutant *SCN1A* using anti-$Na_v1.1$ antibody. Wildtype shows strong bands (two replicates) while the mutant shows little or no labeling above the mock-transfected control. α tubulin is the loading control. (F) Densitometric quantification of $Na_v1.1$ immunoblots from several separate cultures normalized to α tubulin expression. *, $p<0.001$, ANOVA with Tamhane´s T2 as post-hoc test.

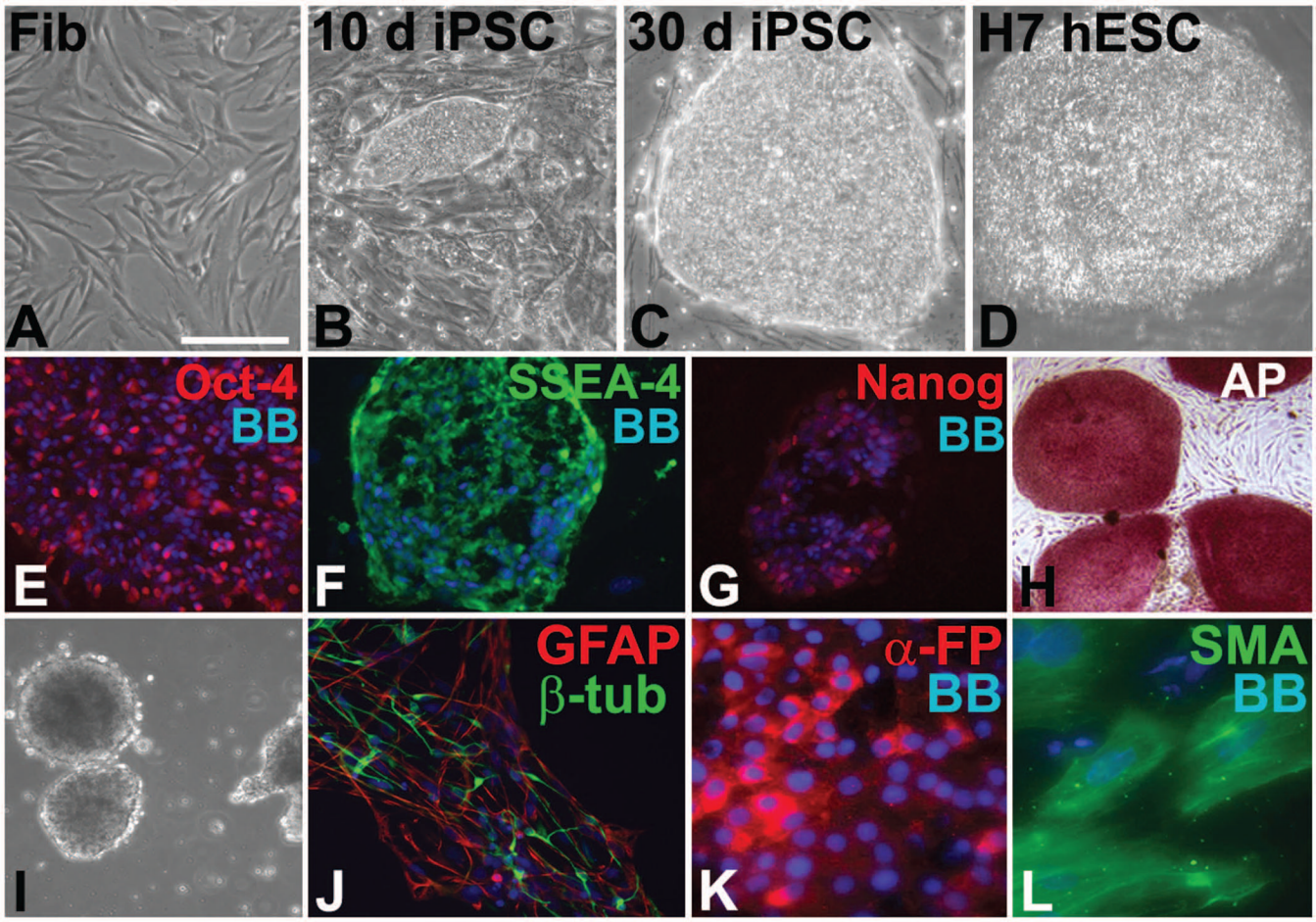

Figure 2.

Reprogramming DS patient fibroblasts into iPSCs. (**a**) Skin biopsy-derived fibroblasts from patient DS1 before reprogramming. (B–D) After 4-factor retroviral reprogramming, pluripotent stem cell colonies began to form within 10 days (B), were well developed by 30 days (C), and their morphology was similar to a hESC colony from the H7 line (D). (E–G) Patient-specific iPSCs expressed pluripotency markers Oct4 (E), stage-specific embryonic antigen-4 (SSEA-4; F), nanog (G) and alkaline phosphatase (AP; H). (I–L) Differentiation of patient-specific iPSCs through EBs (I) led to tissue of ectodermal (J), endodermal (K), and mesodermal (L) lineages. β-tub, neuron-specific β-tubulin; GFAP, glial fibrillary acidic protein; α-FP, α-fetoprotein; SMA, smooth muscle actin. Bisbenzimide (BB) nuclear stain is blue in E–G and J–L. Scale bar, 100 μm for A–G; 200 μm for H–J; 50 μm for K, L.

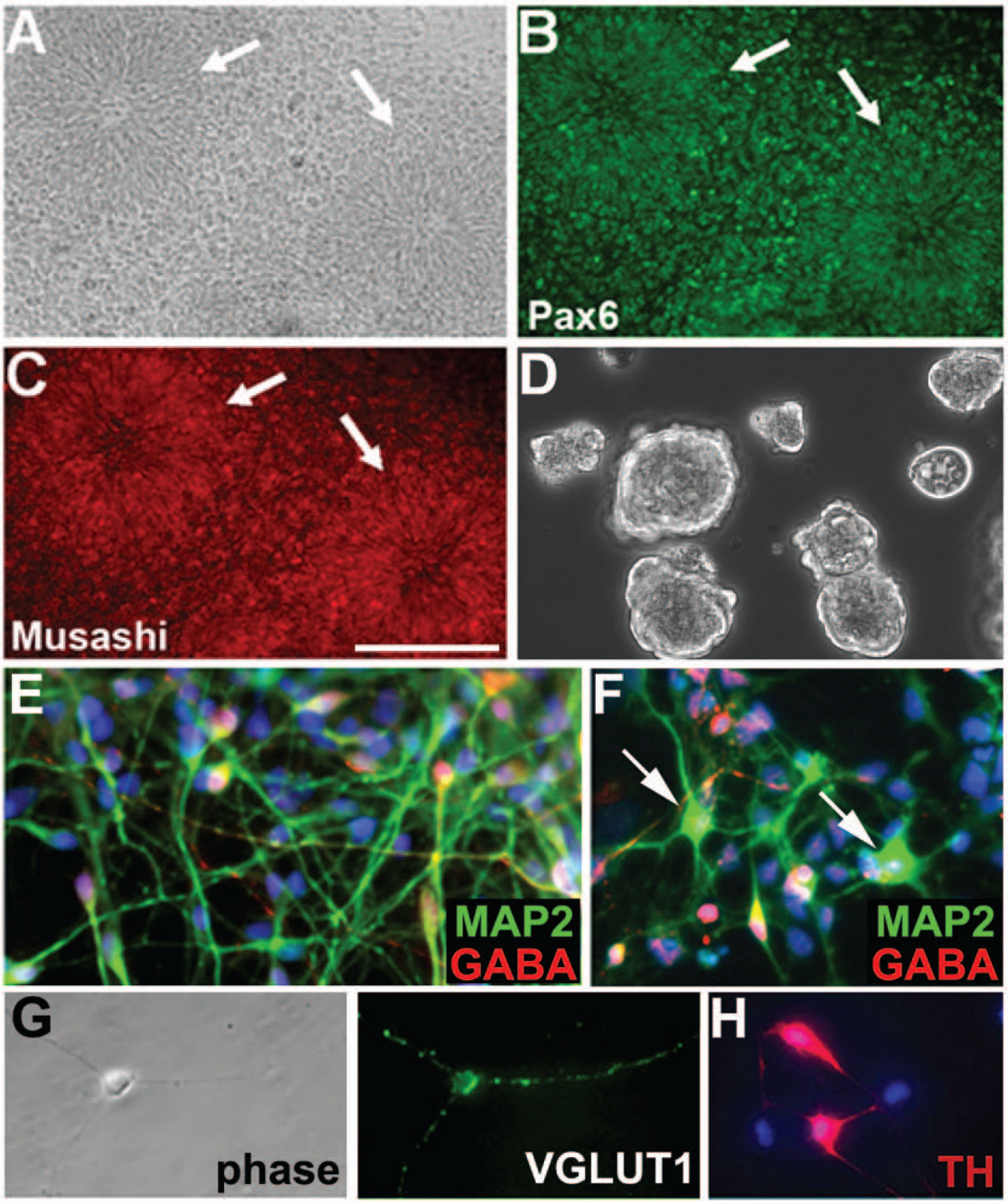

Figure 3.
Neuronal differentiation of DS patient-specific iPSCs. (A–D) Mutant iPSCs were differentiated into neural rosettes (arrows in A–C) that expressed the NPC markers Pax6 (B) and Musashi (C), and then were expanded as neurospheres (D). (**e–g**) Differentiation of iPSC-derived NPCs into MAP2+ (green in E, F) induced neurons yielded mostly GABAergic interneurons (red in E, F), and about 10% pyramidal shaped neurons (arrows in **f**) that expressed the vesicular glutamate transporter-1 (VGLUT1) (G); phase image is shown in the left-hand panel of (G). (H) Rare cells expressed tyrosine hydroxylase (TH).

Bisbenzimide (BB) nuclear stain is blue in E, F, H. Scale bar, 200 μm for A–C; 100 μm for D; 75 μm for E–H.

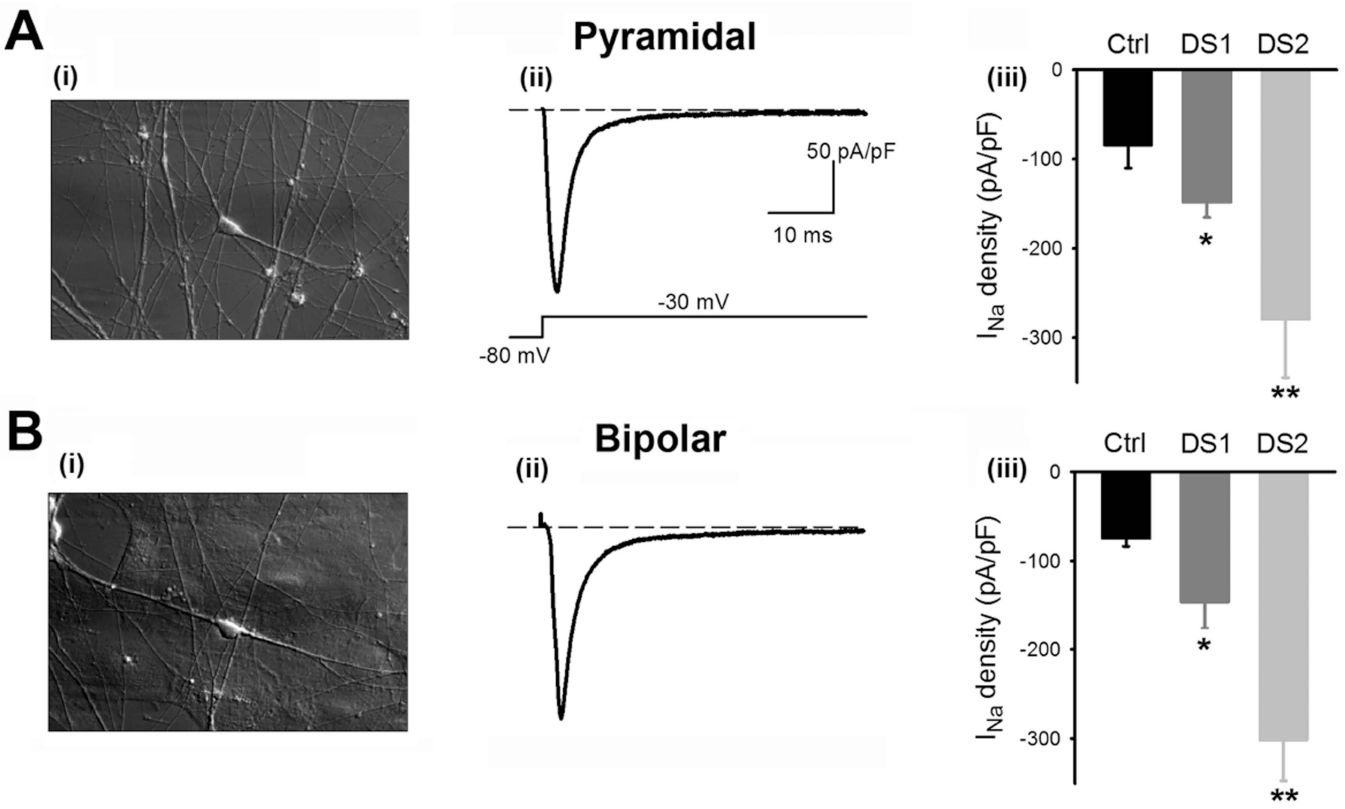

Figure 4.

Sodium current (I_{Na}) density is increased in pyramidal and bipolar neurons with the *SCN1A* mutation. (A, B) Induced neurons with pyramidal (A) or bipolar (B) morphology are shown in phase images on the left (i). Representative traces of I_{Na} (ii) recorded using the protocol displayed in the inset are shown, as are bar graphs of the mean I_{Na} density from control and DS1 and DS2 mutant pyramidal neurons (Aiii; Control: Black bars, n = 14; DS1: Dark gray bars, n = 22; p = 0.012 vs. control. DS2: Light gray, n = 6; p = 0.023 vs. control) and bipolar neurons (Biii; Control, n = 25; DS1, n = 27; p = 0.048 vs. control. DS2, n = 5; p = 0.001 vs. control). *, $p < 0.05$; **, $p < 0.01$. No significant differences in sodium current densities are present between bipolar and pyramidal neurons within groups (p=0.70 and 0.94 for control and DS1, respectively). Error bars indicate means ± s.e.m.

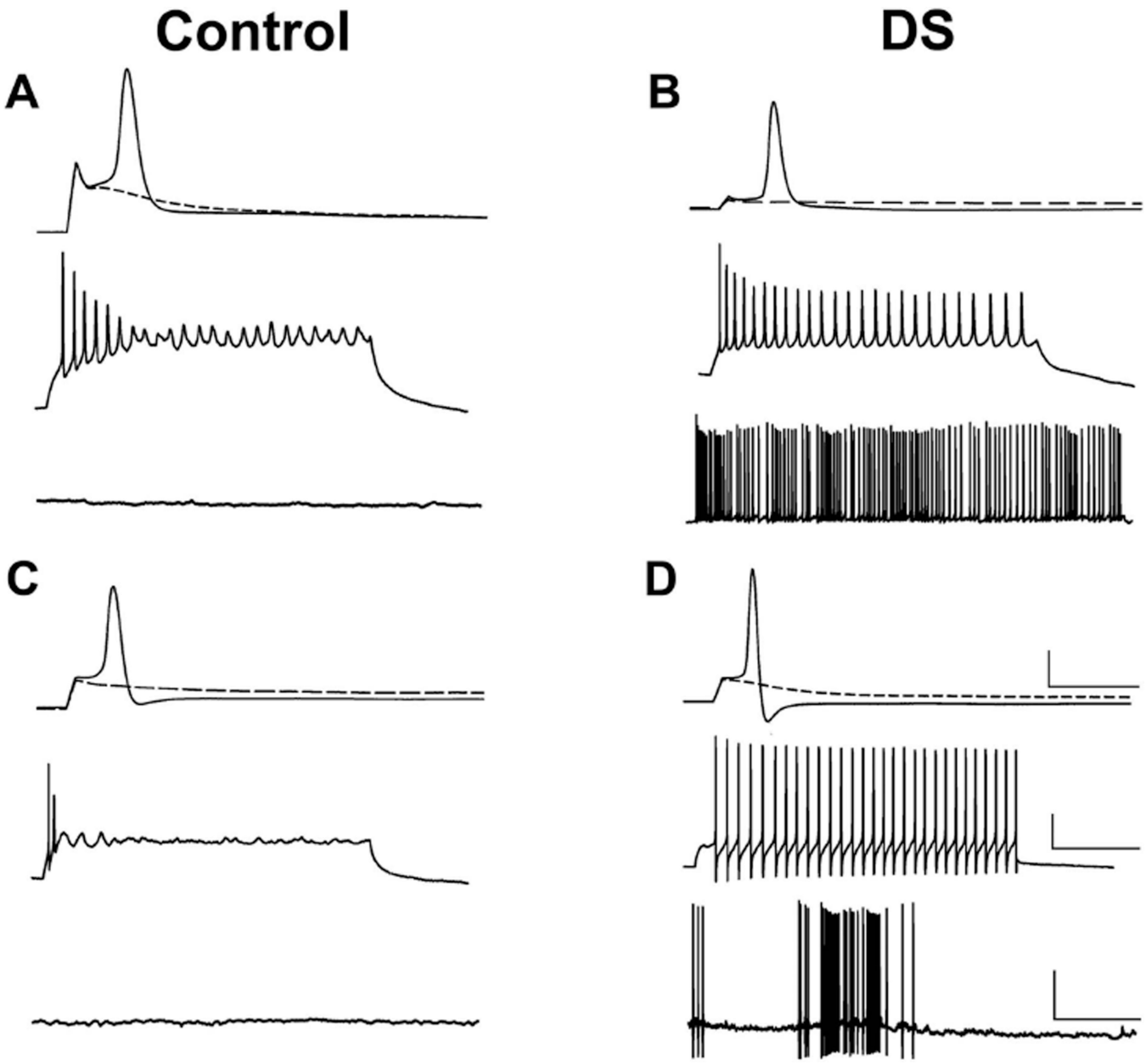

Figure 5.

Characteristics of evoked action potentials (APs) and spontaneous firing in human induced neurons from control and DS subjects. Top Trace in A–D: Representative APs (solid lines) recorded from control (A) or DS2 (B) bipolar-shaped cells or control (C) or DS1 (D) pyramidal-shaped cells cultured for 5 weeks using whole cell patch-clamp recording in current-clamp mode. APs evoked by injection of threshold depolarizing currents required much less current for the DS2 bipolar (B; 0.17 nA, 1 ms) or DS1 pyramidal (D; 0.27 nA, 1 ms) induced neurons than for the control bipolar (A; 0.61 nA, 1 ms) or pyramidal (C; 0.35 nA, 1 ms) induced neurons; cells were held at resting membrane potential (−65 mV for the control bipolar; −63 mV for control pyramidal cells; −55 mV for DS2 bipolar and −72 mV for DS1 pyramidal cells, respectively). Also shown are the responses evoked by subthreshold depolarizing current injections in the same cells (dotted lines of the top traces in A–D). Middle traces in A–D: Repetitive firing evoked by injection of a long-pulse

depolarizing current (0.02 nA, 1500 ms) in the same cells as in the top traces. Note the higher frequency and more prolonged firing in the DS1 or DS2 induced neurons (B, D) than in the controls (A, C). Bottom traces in A–D: No spontaneous firing was observed in either control bipolar (A) or pyramidal (C) induced neurons when held at resting membrane potential, but both DS1 and DS2 patient-specific induced neurons displayed consistent, spontaneous firing with bursting activity at resting membrane potential (B, D). Each trace is a representative example of 7–45 individual cells. Scale bars: 40 pA for all vertical bars; 10 ms, 400 ms and 10 sec for horizontal bars of the top, middle and bottom traces of each panel.

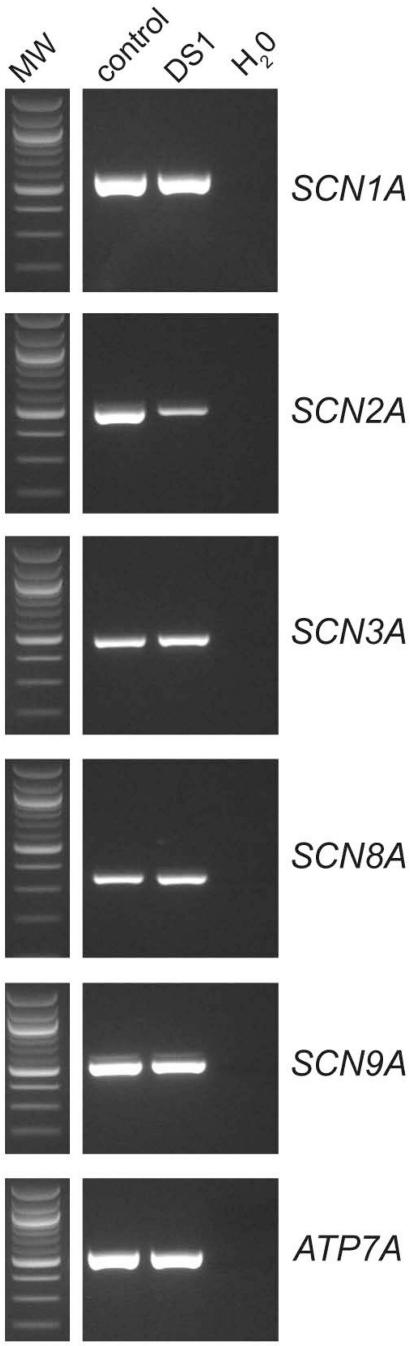

Figure 6.
Sodium channel transcripts in iPSC derived neurons. Total RNA was isolated from induced neurons (5 week) from DS1 and control and amplified by RT-PCR using gene-specific primers (Supplementary Table 1) for five sodium channel genes, as indicated. Transcript abundance is not increased in the patient neurons.

Table 1

Comparisons of passive and evoked membrane electrical properties of bipolar- and pyramidal-shaped induced neurons between control and DS patients.

Group	Resting V_m (mV)	Input Resistance (GΩ)	$V_{Threshold}$ (mV)	AP Amplitude (mV)	AP Frequency (Hz)
B-Ctrl	−67.15 ± 1.37 (33)	1.25 ± 0.15 (33)	−23.67 ± 1.51 (30)	114.90 ± 4.69 (34)	3.48 ± 0.73 (27)
B-DS	−58.55 ± 1.28** (45)	1.24 ± 0.12 (45)	−30.83 ± 1.53** (37)	121.18 ± 3.26 (37)	11.6 ± 1.33** (37)
P-Ctrl	−63.05 ± 2.72 (9)	1.02 ± 0.34 (9)	−20.51 ± 3.37 (8)	125.38 ± 5.14 (8)	5.10 ± 2.66 (7)
P-DS	−58.08 ± 1.24 (31)	1.02 ± 0.17 (31)	−37.32 ± 1.51** (26)	114.35 ± 3.97 (26)	12.64 ± 1.99* (24)

Values are mean ± SEM; cell numbers in parentheses.

Abbreviations: Resting Vm, resting membrane potential; $V_{Threshold}$, threshold membrane potential for evoking an action potential (AP); AP Amplitude, Spike height measured from the resting membrane potential level to the peak; AP Frequency, the frequency of repetitive firing of a given iPSC in response to injection of a 1500 ms depolarizing current pulse (0.02 nA); B-Ctrl, bipolar-shaped neurons from control iPSCs; B-DS, bipolar-shaped neurons from DS iPSCs; P-Ctrl, pyramidal-shaped neurons from conrol iPSCs; P-DS, pyramidal-shaped neurons from DS iPSCs.

* $p<0.05$;

** $P < 0.001$,

Student's *t* test or Mann-Whitney Rank Sum test.

Table 2

Induced neurons from DS patients, but not controls, often display spontaneous bursting behavior/repetitive firing at resting membrane potential.

iPSCs	Control (%)	DS patient (%)
Pyramidal-shaped	0 (0/7)	68 (19/28)
Bipolar-shaped	4 (1/27)	49 (18/37)
Overall	3 (1/34)	57 (37/65)